BIOCELL

Tech Science Press

Doi:10.32604/biocell.2025.062137

ARTICLE

Picropodophyllotoxin: A Natural Epimer Targeting STAT3 Phosphorylation and ROS-Mediated Apoptosis in Oral Squamous Cell Carcinoma Cells

Jung-Il Chae[1,#], Ji-Hye Seo[1,#], Goo Yoon[2], Young-Joo Jeon[3,*] and Woo-Keun Kim[4,*]

[1]Department of Dental Pharmacology, School of Dentistry, Jeonbuk National University, Jeonju, 54896, Republic of Korea
[2]Department of Pharmacy, College of Pharmacy, Mokpo National University, Muan, 58554, Republic of Korea
[3]Disease Target Structure Research Center, Korea Research Institute of Bioscience and Biotechnology (KRIBB), Daejeon, 34141, Republic of Korea
[4]Biosystem Research Group, Department of Predictive Model Research Center, Korea Institute of Toxicology, Daejeon, 34114, Republic of Korea

*Corresponding Authors: Young-Joo Jeon. Email: jeonyj@kribb.re.kr; Woo-Keun Kim. Email: wookkim@kitox.re.kr

#These authors contributed equally: Jung-Il Chae and Ji-Hye Seo

Received: 11 December 2024; Accepted: 28 March 2025; Published: 30 April 2025

ABSTRACT: Background: Picropodophllotoxin (PPT), a principal component of *Podophyllum hexandrum* root, demonstrates various beneficial biological activities in multiple cancer types, including antitumor and antiproliferative properties. Despite its known effects, the specific mechanisms by which PPT induces apoptosis in oral squamous cell carcinoma (OSCC) cells lack full clarification. **Aims:** This study aimed to evaluate the role of PPT in inducing apoptosis in OSCC cells by targeting signal transducer and activator of transcription 3 (STAT3) and to investigate the underlying molecular pathways. **Methods:** Human OSCC cell lines (HN22 and HSC4) were treated with PPT. Cell viability, colony formation, and apoptotic morphological changes were evaluated. Reactive oxygen species (ROS) generation and mitochondrial function were assessed using tetramethyl rhodamine methyl ester, MitoSOX, and 2′, 7′-dichlorodihydrofluorescein diacetate (DCFH-DA) assays following PPT treatment. The expression of apoptosis markers, including cleaved Poly (ADP-Ribose) Polymerase (c-PARP) and other target proteins, was measured using western blotting. ROS involvement was further confirmed using the ROS scavenger N-acetylcysteine (NAC). **Results:** Treatment with PPT resulted in a substantial reduction in cell viability, a decrease in colony formation capacity, and evident morphological changes in OSCC cells. These effects were dose- and time-dependent, as evidenced by increased expression of c-PARP. PPT-induced apoptosis was mediated by excessive ROS generation, which was almost completely blocked by NAC pretreatment. **Conclusions:** These findings suggest that PPT may serve as a promising therapeutic agent for treating human oral cancer by inhibiting the STAT3 pathway and inducing ROS-mediated apoptosis.

KEYWORDS: Picropodophyllotoxin; STAT3; ROS; oral squamous cell carcinoma; apoptosis

1 Introduction

Oral squamous cell carcinoma (OSCC) is a common type of malignant tumor that arises from the oral mucosa and represents the seventh most common cancer type worldwide among various malignancies [1]. GLOBOCAN 2020 reported 377,713 newly diagnosed cases of OSCC and 177,757 deaths worldwide. The incidence and mortality rates are higher in males than in females and are projected to increase further [2,3]. OSCC development is strongly associated with lifestyle-related factors such as excessive alcohol consumption, smoking, and immune deficiency disorders. Chronic exposure to these factors promotes the progression

of malignant tumors [4]. Despite advancements in chemotherapy, radiation therapy, and immunotherapy, the prognosis of patients with OSCC remains poor, owing to late detection and diagnosis, with a 5-year survival rate as low as 50% [5,6]. Therefore, there is an urgent need for novel therapeutic agents that target key molecular pathways to improve treatment outcomes.

Picropodophyllotoxin (PPT) is a structural isomer of podophyllotoxin and is classified as a cyclolignan. This compound is naturally derived from the roots of *Podophyllum hexandrum*. Programmed cell death, commonly referred to as apoptosis, is a critical mechanism for removing damaged or unnecessary cells, thereby ensuring tissue homeostasis. In cancer, apoptosis is often disrupted, enabling tumor cells to evade destruction and proliferate uncontrollably. As such, therapeutic strategies targeting apoptotic pathways have become a key focus in cancer research [7,8]. Recent studies demonstrated that PPT exhibits anticancer activity by inducing apoptosis and inhibiting the G1 and G2/M cell cycles in diverse malignant tumor types, including non-small cell lung cancer, colon cancer, and esophageal squamous cell carcinoma [9–11]. These findings suggested that PPT induces apoptosis through its bioactive properties. Despite its promising anticancer potential, the specific molecular mechanisms by which PPT exerts its effects in OSCC, particularly in HN22 and HSC4 cell lines, remain unclear and warrant further investigation.

Transcription factors (TFs) are key regulators of gene expression that bind to specific DNA sequences and control various biological processes such as cell division, survival, and apoptosis [12]. The human genome contains approximately 1600 TFs [13], and the activation or inhibition of these TFs influences their key cellular functions [14]. Dysfunctional TF regulation and mutations in the TF-binding sites have been linked to several human diseases [15]. One such transcription factor, Signal Transducer and Activator of Transcription 3 (STAT3) is a member of the STAT family (STAT1–STAT6). STAT3 is activated through the phosphorylation of its tyrosine 705 and serine 727 residues, and tyrosine phosphorylation is particularly critical for its activation [16,17]. Once activated, phosphorylated STAT3 regulates the expression of genes involved in cell survival and proliferation, either through nuclear translocation or other signaling mechanisms. STAT3 is implicated in oncogenesis through the regulation of key regulators of cell survival, namely Bcl-2, Mcl-1, survivin, and cyclin D1 [18]. Persistent activation and overexpression of STAT3 have been observed in various solid tumors, including lung [19], breast [20], gastric [21,22], and colorectal cancers [23,24]. Therefore, targeting the STAT3 signaling pathway is considered a promising therapeutic strategy for preventing tumor progression. This study sought to explore the anticancer potential of PPT in OSCC cells by examining its role in STAT3 inhibition and apoptosis induction, suggesting its potential as a novel therapeutic agent.

2 Materials and Methods

2.1 Cell Lines and Reagents

The cells (HN22 and HSC4) were obtained from Hokkaido University (Hokkaido, Japan). Dulbecco's modified Eagle's medium (DMEM, Gibco, 11965092), fetal bovine serum (FBS, Gibco, 16000044), penicillin and streptomycin (P/S, Gibco, 15140122), 0.05% trypsin-EDTA (Gibco, 15400054), and phosphate-buffered saline (PBS, Gibco, 10010023) were purchased from Thermo Fisher Scientific, Inc. (Waltham, MA, USA). Picropodophyllotoxin (PPT; PubChem CID: 72435) was purchased from Sigma-Aldrich (St. Louis, MO, USA). 3-(4,5-dimethylthiazol-2-yl)-2,5-diphenyl tetrazolium bromide (MTT) was purchased from Duchefa (M1415, Haarlem, the Netherlands). 4′,6-diamidino-2-phenylindole (DAPI), and UltraCruz mounting medium were purchased from Santa Cruz Biotechnology (sc-24941, Dallas, TX, USA). 2′,7′-dichlorodihydrofluorescein diacetate (DCFH-DA) was purchased from Invitrogen (D399, Invitrogen Corp., Carlsbad, CA, USA). Basal Medium Eagle (BME) was purchased from Sigma-Aldrich, Inc. (B9638, St. Louis, MO, USA). N-Acetyl-L-cysteine (NAC) was purchased from Sigma-Aldrich (A7250-10G, St. Louis, MO, USA). Colivelin, a STAT3 activator, was purchased from Selleckchem (S9664, Houston, TX, USA). A

phosphatase inhibitor cocktail solution (100X) was purchased from GenDEPOT (P3200-001, Katy, TX, USA). The primary antibodies against Stat3(sc-483), Bcl-2(sc-7382), caspase3(sc-7148), GAPDH(sc-166545), and β-actin(sc-47778) were sourced from Santa Cruz Biotechnology, Inc. (Santa Cruz, CA, USA). Antibodies targeting PARP(#9542), p-STAT3(#9145S), Mcl-1(#4592), survivin(#2808), Bax(#5023), BIM(#2933), and c-caspase3(#9664) were obtained from Cell Signaling Technology (Danvers, MA, USA). AB clonal Biotech Co., Ltd. (Woburn, MA, USA) provided the primary antibodies against c-caspase3(ab32042). The secondary antibodies, goat anti-mouse IgG-HRP and goat anti-rabbit IgG-HRP were purchased from Santa Cruz Biotechnology, Inc. (sc-2005, Santa Cruz, CA, USA) and BETHYL (A120-101P, Seoul, Republic of Korea), respectively. Mycoplasma removal agent (MRA) was purchased from MP Biomedicals (cat#3050044, Irvine, CA, USA). The anti-infective solution was supplied by DoGenBio (cat#DG-AIS500, Seoul, Republic of Korea).

2.2 Cell Culture

The HN22 and HSC4 human OSCC cells were maintained in DMEM supplemented with 10% heat-inactivated FBS and 100 U/mL penicillin/streptomycin (P/S) and incubated at 37°C in a humidified atmosphere containing 5% CO_2. The incubation duration was either 24 or 48 h unless otherwise specified. We confirm that all cell lines used in this study were treated with MRA at the manufacturer's recommended concentration (0.1 μg/mL) to prevent mycoplasma contamination. Additionally, an anti-infective solution was applied to the water bath (2000-fold dilution), the humidity chamber of the CO_2 incubator (1000-fold dilution), and the surfaces of various equipment and instruments (200-fold dilution with 70% ethanol) to further ensure a contamination-free environment.

2.3 MTT Cytotoxicity Assay

To measure cytotoxicity, HN22 cells (2000 cells/well) and HSC4 cells (2500 cells/well) were seeded in flat-bottomed 96-well plates and treated with various doses (125, 250, 500, and 1000 nM) of PPT for different times (24 and 48 h), respectively. Subsequently, 20 μL of 5 mg/mL MTT solution was added to each well and incubated for 1 h 30 min. After discarding the MTT solution, 200 μL of dimethylsulfoxide (DMSO) was added to each well, and the absorbance was measured at 540 nm using the Epoch^{TM} microplate spectrophotometer (BioTek Instruments, Inc., Winooski, VT, USA).

2.4 DAPI Staining

To evaluate the effect of the target drug (PPT), DAPI staining was performed. First, cells treated with PPT were collected using 0.05% trypsin-EDTA, washed twice with 1X phosphate-buffered saline (PBS), and fixed with 100% methanol for 20 min at room temperature (RT). After removing the methanol, the cells were transferred to a glass slide and mounted using an aqueous mounting medium containing DAPI (Ultracruz Mounting Medium, Santa Cruz, CA, USA). Finally, the samples were analyzed using an Olympus IX73-DP73 microscope (Olympus Corp., Shinjuku, Tokyo, Japan).

2.5 Anchorage-Independent Cell Growth Assay

A 0.5% agar-BME medium (with FBS, gentamicin, L-glutamine, and PBS) was prepared and poured as the bottom layer into a 6-well plate, 3 mL per well. After solidification, 1 mL/well of the same components in BME medium containing each cell line (8000 cells/well) and PPT were dispensed onto the upper layer. Two weeks later, each colony was photographed using a light microscope Olympus IX73-DP73 (Olympus Corp., Shinjuku, Tokyo, Japan). The colonies were then compared with the negative control (DMSO only), and the experiment was repeated three times.

2.6 ROS Staining Assay

By using DCFH-DA (Molecular Probes), intracellular ROS accumulation was measured. Each cell type (HN22 and HSC4) was seeded at a density of 1×10^5 cells/well and 1.2×10^5 cells/well, respectively, in a 4-well plate, pretreated with or without NAC, followed by treatment with DMSO and PPT (125, 250, and 500 nM) for 24 h. Treated cells were washed twice with PBS solution and reacted with 20 μM DCFH-DA for 30 min at 37°C in a 5% CO_2 incubator. After removing the dye and washing with PBS, the cells were finally stained with DAPI. Cellular fluorescence was observed under a fluorescence microscope (Olympus Corp., Shinjuku, Tokyo, Japan).

2.7 Western Blotting

Following treatment with PPT on HN22 and HSC4 cells, at the end of the 48 h treatment period, each cell sample was harvested using a 0.05% Trypsin-EDTA, washed twice with cold 1X PBS, and centrifuged at 3000 rpm (Fresco^{TM}17, Thermo Fisher Scientific, USA) for 3 min at 4°C. Total cell lysates were obtained using RIPA lysis buffer (89900, Thermo Fisher Scientific) containing protease inhibitor/phosphatase inhibitors, and the extracted proteins were quantified using a BCA protein assay kit (23227, Thermo Fisher Scientific). Equal amounts of protein per lane were separated by 8%–12% SDS-polyacrylamide gel electrophoresis and transferred onto a polyvinylidene fluoride (PVDF) membrane (ISEQ00010, Millipore, Burlington, MA, USA). The membranes were blocked with 5% non-fat milk in 1X TBS containing 0.1% Tween 20 (TBST) for 1 h at RT to reduce non-specific binding. To allow the membranes to react with specific primary antibodies (dilution range of 1:1000 to 1:2000 for p-STAT3, STAT3, c-caspase3, caspase3, PARP, Mcl-1, survivin, Bcl-2, Bax, Bim, GAPDH, β-actin), they were incubated overnight at 4°C in 1X TBST containing the antibodies. The bound antibody membranes were washed three times for 10 min each with 1X TBST and then incubated with secondary antibodies conjugated to horseradish peroxidase (HRP) (Santa Cruz Biotechnology, USA) at a dilution range of 1:5000 to 1:10,000 for 2 to 3 h at room temperature, depending on the specific antibody used. The membranes were visualized using the ImageQuant LAS4000 Mini system (GE Healthcare Life Sciences, Chalfont, UK) with an enhanced chemiluminescence (ECL) reagent (BWP0400, Guri-si, Republic of Korea).

2.8 Flow Cytometry Analysis

A total of 300,000 cells/well were seeded into a 12-well culture microplate. PPT was added to the OSCC cell culture medium at concentrations of 250, 500, and 1000 nM for 48 h. For analysis, cells were subjected to enzymatic treatment with 0.05% trypsin-EDTA for 3 min to obtain single-cell suspensions. In apoptosis assays, fluorescein-tagged Annexin V (556547, BD Pharmingen^{TM}, San Jose, CA, USA) and 7-amino-actinomycin D (559925, BD Pharmingen^{TM}, San Jose, CA, USA) were used to stain the cells. For detecting superoxide and ROS, the cells were incubated with MitoSOX^{TM} Red mitochondrial superoxide indicator (M36008, Thermo Fisher Scientific) for 10 min at 37°C. For mitochondrial membrane potential, the cells were stained with 100 mM tetramethyl rhodamine methyl ester (TMRM) (T668, Invitrogen, Waltham, MA, USA) for 30 min at 37°C and analyzed using BD FACSCerse (BD Biosciences, San Jose, CA, USA). Data were analyzed using FlowJo^{TM}v10 software (BD Bioscience, San Jose, CA, USA).

2.9 Statistical Analysis

For the results derived from the experiment, statistically significant differences were determined using Student's *t*-test. The experiment was performed in three independent replicates (n = 3), where the entire procedure, including cell treatment, incubation, and analysis, was conducted separately three times under

the same conditions. The *p*-values were visualized as "*", "**", and "***" for $p < 0.05$, $p < 0.01$, and $p < 0.001$, respectively, to indicate statistical significance.

3 Results

3.1 PPT Treatment Suppresses Cell Proliferation in OSCC Cells

The molecular structure of PPT is depicted in Fig. 1A. Cytotoxicity screening is essential for analyzing molecular mechanisms. Therefore, we first evaluated the viability of HN22 and HSC4 cells using the MTT assay to confirm the anti-proliferative effect of PPT. PPT suppressed cell proliferation in a concentration- (125, 250, 500, and 1000 nM) and time-dependent (24 and 48 h) manner. The half-maximal inhibitory concentration (IC_{50}) values after 48 h of treatment were 217 nM for HN22 cells and 683 nM for HSC4 cells, respectively (Fig. 1B,C). Additionally, as the concentration of PPT increased, the overall cell count decreased, owing to the loss of cell adhesion compared to that in the control group (Fig. 1D). To evaluate the tumor-selective cytotoxicity of PPT, we conducted MTT assays using HaCaT cells, a well-established non-tumorigenic keratinocyte model in OSCC research. HaCaT cells have been validated as a reliable system for distinguishing the cytotoxic effects of compounds on tumor and non-tumor cells [25,26]. Our results showed that PPT exhibited significantly lower cytotoxic effects on HaCaT cells than on HN22 and HSC4 cells (data not shown). These findings indicate that PPT induces cytotoxicity primarily in OSCC cells while sparing non-tumor cells, highlighting its potential role in suppressing cancer cell growth.

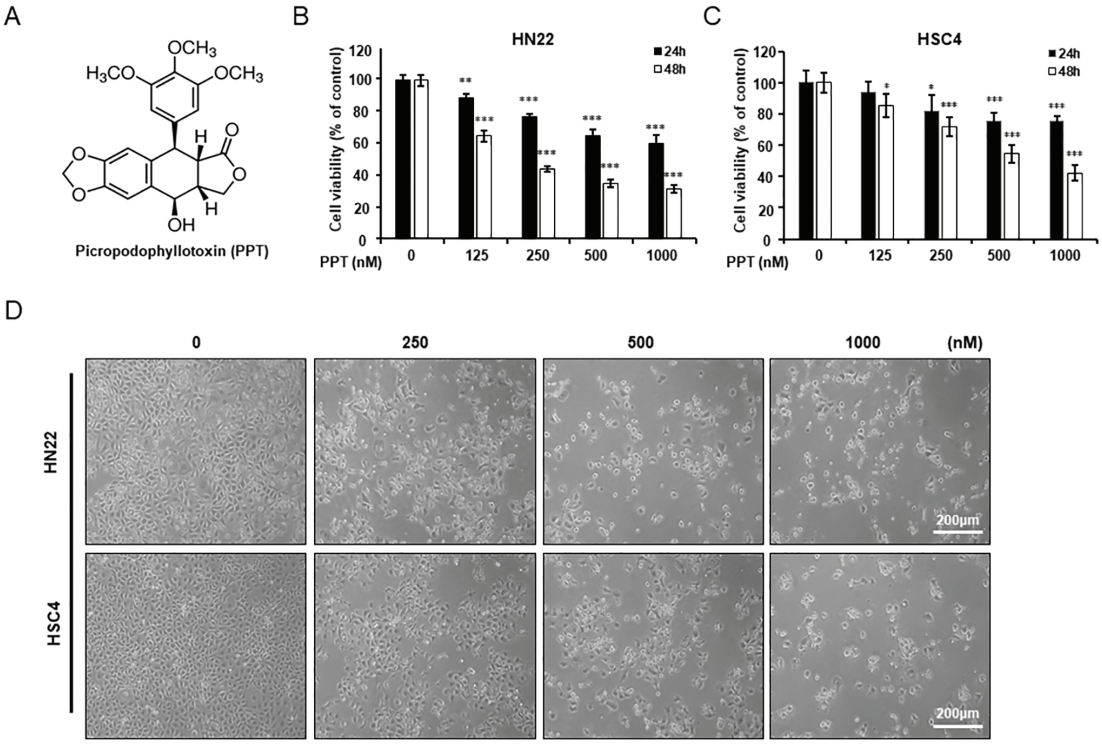

Figure 1: Differential cytotoxic ability of PPT in OSCC cells. (A) Chemical formula structure of PPT. (B,C) Treatment of PPT (125, 250, 500, and 1000 nM) for 24 h, and 48 h in HN22 and HSC4 cells, and the cell viability was measured by MTT assay. Data were expressed as the mean ± SD from independent triplicate experiments (n = 3). The asterisks (*) marked statistical significance (*$p < 0.05$, **$p < 0.01$, ***$p < 0.001$). (D) After exposure to various doses (0, 250, 500, and 1000 nM) of PPT, HN22, and HSC4, cell morphology changed at 48 h post-treatment. DMSO was applied to the control cells as a vehicle treatment (Magnification: 4×) (scale bar = 200 μm)

3.2 PPT Leads to Apoptosis and Inhibition of Colony Formation in OSCC Cells

Next, we used flow cytometry to determine whether PPT induces apoptosis in OSCC cells. As shown in the quadrant plot, the number of early apoptotic cells gradually increased with increasing PPT concentration (Fig. 2A,B). The quadrants were as follows: live (lower left), early apoptotic (lower right), late apoptotic or dead (upper right), and necrotic or dead cells (upper left). Consistent with these findings, PPT treatment at a concentration above 500 nM significantly increased apoptotic cells, as demonstrated by more prominent nuclear condensation and DNA fragmentation observed in DAPI-stained images (Fig. 2C). These apoptotic morphological features were quantified through visual inspection of DAPI-stained images. The bar graph (Fig. 2D) illustrates a significant dose-dependent rise in apoptotic cell proportion. As shown in Fig. 2E,F, PPT treatment significantly reduced the colony-forming ability of both HN22 and HSC4 cells at concentrations exceeding 125 nM. The number and size of the colonies were markedly smaller than those in the control group. Quantitative analysis further supported these observations, showing a significant reduction in the percentage of colonies relative to that of the control. These findings indicated that PPT induces apoptosis and suppresses the clonogenic potential of OSCC cells, demonstrating its effectiveness in impeding cancer cell proliferation.

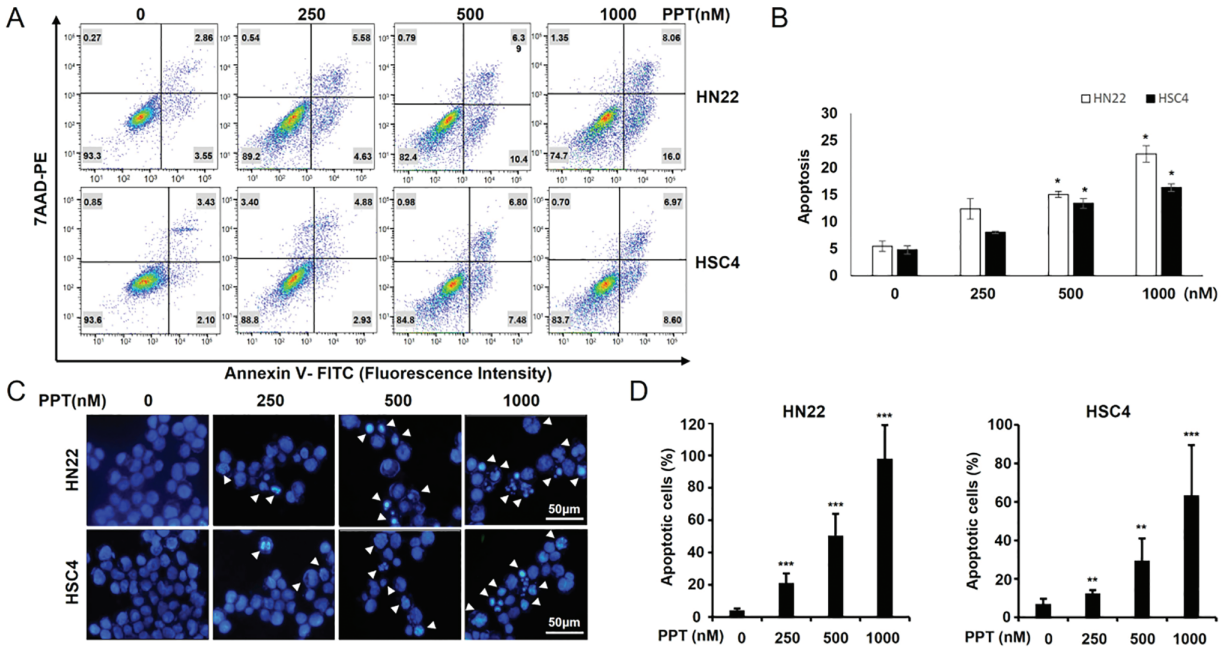

Figure 2: (Continued)

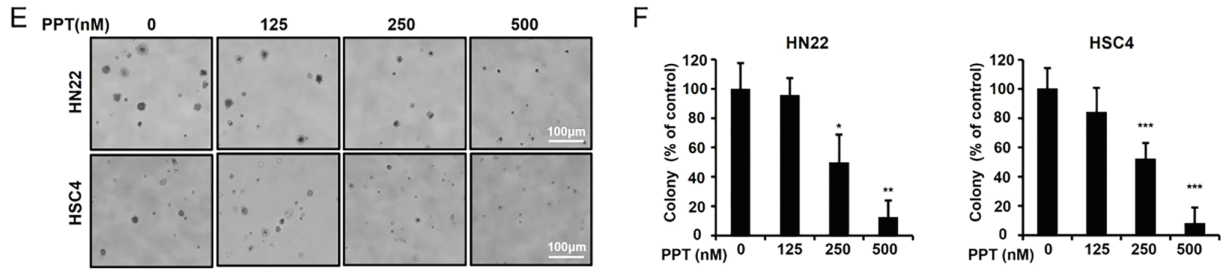

Figure 2: Induction of apoptosis and inhibition of colony forming by PPT in OSCC cells. (A) PPT-induced apoptotic cell death was analyzed using the Annexin V/7-AAD staining. (B) Quantitative data showing the percentage of apoptotic cells according to treatment. The results are presented as the mean ± SD from three independent experiments (n = 3). Statistical significance is indicated by asterisks (*), with $p < 0.05$. (C,D) HN22 and HSC4 cells, after treatment with PPT (250, 500, and 1000 nM) for 24 h, were analyzed using DAPI staining and then visualized using a fluorescence microscope under 20× (scale bar = 50 μm). White arrows indicate apoptotic cells with nuclear condensation and fragmentation, characteristic of apoptosis, and the bar graph quantifies apoptotic cells from DAPI-stained images by visual inspection. The asterisk (*) marked statistical significance (*$p < 0.05$ **$p < 0.01$, ***$p < 0.001$). The values showing the means of independent triplicate experiments ± SD. (E,F) Colony forming inhibitory effect of PPT on HN22 and HSC4 cells at varying doses. The bar graph was quantified for the number of colonies in HN22 and HSC4 cells after treatment with PPT (125, 250, and 500 nM). The values were obtained from three separate experiments and expressed as the mean ± SD (n = 3). The asterisks (*) marked statistical significance (*$p < 0.05$, **$p < 0.01$, ***$p < 0.001$). The pictures were taken at 100× magnification using an Olympus IX73-DP73 microscope (scale bar = 100 μm)

3.3 PPT Induces Mitochondrial Dysfunction and ROS Generation in OSCC Cells

Mitochondria are key organelles in cellular energy metabolism that play a critical role in regulating cell death and generating ROS. Therefore, we hypothesized that the induction of cell death by PPT in OSCC cells might be associated with ROS production, leading us to perform a MitoSOX analysis. The results revealed that intracellular ROS levels in HN22 and HSC4 cells increased progressively with increasing PPT concentration (Fig. 3A,B). TMRM is a fluorescent dye used to measure mitochondrial membrane potential (Δψm). Under normal conditions, a high Δψm causes TMRM to accumulate inside mitochondria, producing high fluorescence. In contrast, damaged or dying cells exhibit a reduced Δψm, resulting in decreased TMRM fluorescence. Our TMRM assay demonstrated that PPT treatment at concentrations of 250, 500, and 1000 nM reduced TMRM fluorescence in both HN22 and HSC4 cells, indicating that PPT weakened mitochondrial membrane potential, leading to mitochondrial dysfunction and apoptosis (Fig. 3C,D). Finally, we performed DCFH-DA assays to evaluate whether the PPT-induced reduction in mitochondrial membrane potential caused by PPT directly contributed to ROS production. As illustrated in Fig. 3E,F, treatment with PPT (125, 250, and 500 nM) caused a dose-dependent increase in ROS levels, which was counteracted by pretreatment with NAC. These results align with prior research findings and further corroborate the idea that PPT induces apoptosis by generating ROS. Therefore, the exposure of OSCC cells to PPT alters the cellular microenvironment. Collectively, our results suggested that PPT induces mitochondrial dysfunction, leading to increased ROS production, which contributes to cell death. Furthermore, as depicted in Fig. 3G, the quantitative assessment revealed a notable, dose-dependent rise in ROS levels in both HN22 and HSC4 cells upon PPT treatment. Moreover, Fig. 3H demonstrates that NAC pretreatment effectively reduced PPT-induced ROS accumulation, further highlighting the critical role of ROS in promoting PPT-driven apoptosis.

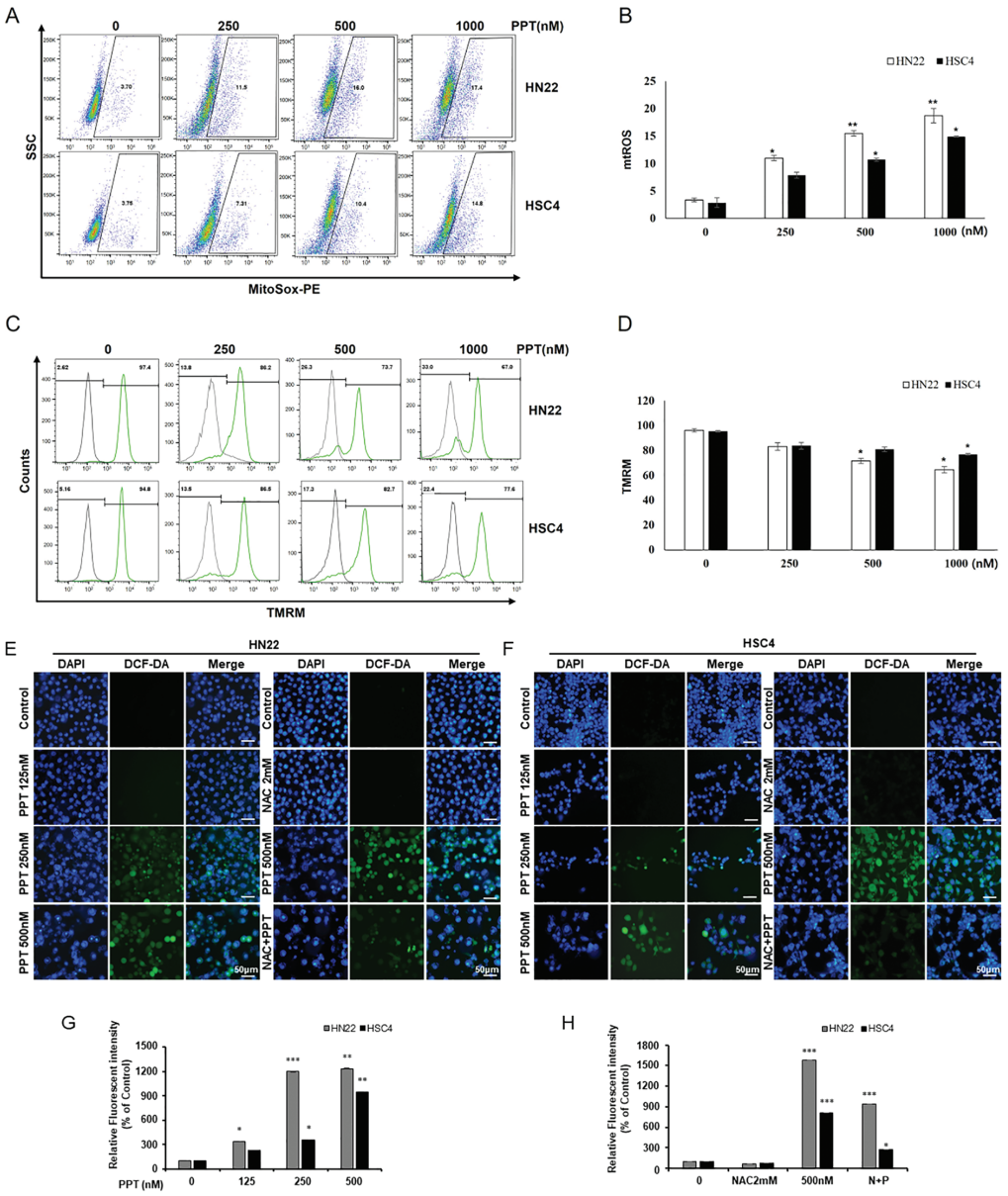

Figure 3: PPT treatment induces Intracellular generation of ROS in OSCC cells. (A) PPT-induced increases in mitochondrial ROS levels were analyzed using MitoSOX-based flow cytometry. (B) Quantitative analysis of MitoSOX fluorescence intensity, indicating the relative mitochondrial ROS levels in HN22 and HSC4 cells. Data are expressed as the mean ± SD (n = 3), and statistical significance was determined as follows: *$p < 0.05$, **$p < 0.01$. (C) The mitochondrial membrane potential was examined via MRM staining and flow cytometry. (D) Quantitative analysis of TMRM fluorescence intensity confirmed a decline in mitochondrial membrane potential in HN22 and HSC4 cells following PPT treatment. This reduction in fluorescence indicates mitochondrial membrane depolarization. Mean ± SD (n = 3) values are depicted, and statistical significance was analyzed using Student's *t*-test, *$p < 0.05$. In HN22 (E) and HSC4 (F) cells, fluorescence intensity was confirmed after 1 h pretreatment with 2 mM NAC, followed by PPT treatment, and ROS levels were measured using DCFH-DA (20 μM) staining. Nuclei were visualized using DAPI staining. The images were taken with an Olympus IX73-DP73 microscope, and a scale bar of 50 μm is shown. (G,H) DCFH-DA fluorescence intensity values were normalized to DAPI fluorescence and calculated as percentages relative to the control. The bar graphs expressed the mean ± SD (n = 3), and statistical significance is shown as follows: *$p < 0.05$, **$p < 0.01$, and ***$p < 0.001$

3.4 PPT Regulates STAT3 and Apoptosis-Linked Protein Expression in OSCC Cells

Among the STAT protein family, STAT3 plays a critical role in promoting tumor growth by enhancing cell survival mechanisms and resisting apoptosis [27,28]. Therefore, the inhibition of the constitutive activation of STAT3 is considered a strategy to combat cancer progression. We examined whether PPT affects STAT3 phosphorylation in HN22 and HSC4 cells using western blotting. Data presented in Fig. 4A indicated that PPT treatment significantly decreased p-STAT3 levels in a dose-dependent manner, whereas total STAT3 protein levels remained unchanged in OSCC cells. Furthermore, Fig. 4B,C shows that PPT treatment enhanced the expression of c-PARP, a key marker of apoptosis, in a dose- and time-dependent manner. Notably, p-STAT3 levels were also reduced in a time-dependent manner, with significant inhibition observed at 24 and 48 h in both HN22 and HSC4 cells (Fig. 4C). This suggests that PPT-mediated STAT3 inhibition is progressive over time, further contributing to apoptotic signaling. Additionally, PPT suppressed anti-apoptotic proteins, including Mcl-1, Bcl-2, and survivin, and upregulated pro-apoptotic factors, such as Bax, Bim, and cleaved caspase-3. These results suggested that PPT facilitates apoptosis by modulating key regulatory proteins, ultimately inducing cancer cell death.

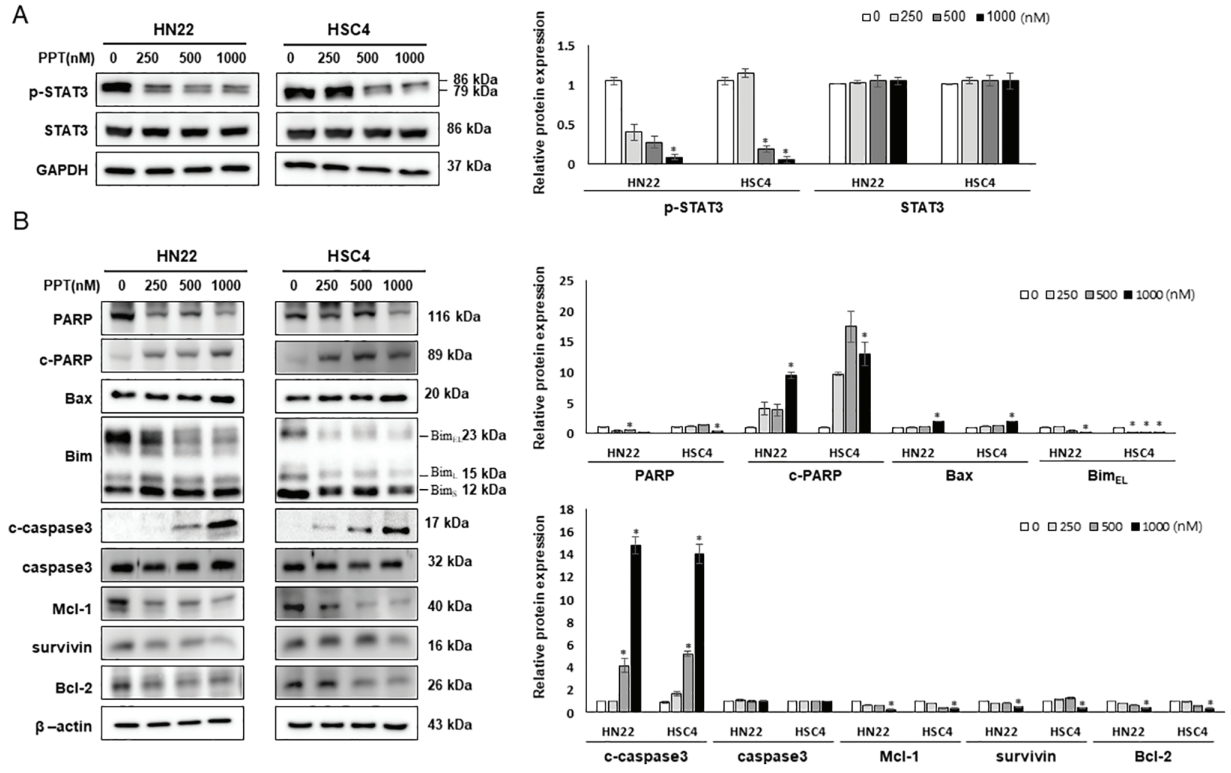

Figure 4: (Continued)

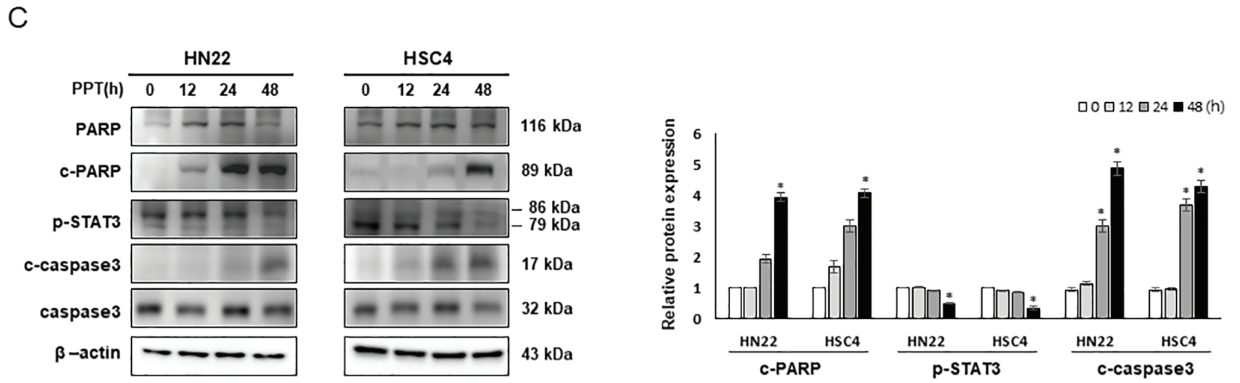

Figure 4: Regulation effect of PPT on STAT3 phosphorylation and downstream protein level in OSCC cells. PPT-treated with differ doses (250, 500, and 1000 nM) in HN22 and HSC4 cells for 48 h. (A) Western blotting for p-STAT3 and STAT3 after treating HN22 and HSC4 cells with PPT for 48 h. Each cell lysates were assessed by quantified to BCA assay to equal loading of proteins. As a loading control was used a GAPDH. (B) Immunoblotting image for PARP, Bax, Bim, c-caspase3, Mcl-1, survivin, Bcl-2 antibodies after HN22 and HSC4 cells incubated with PPT or DMSO for 48 h. Beta-actin protein bands were used as the loading control. (C) Samples were obtained in a time-dependent manner with 500 nM of PPT treating for each cell, and expression levels of c-PARP, p-STAT3, c-caspase3, and total PARP, caspase3 were verified via western blotting. β-actin protein bands were used for loading normalization. A bar graph depicts the normalized relative protein levels compared to the loading control across various treatment groups, presented as the mean ± SD (n = 3), with statistical significance marked as follows: $^{*}p < 0.05$

3.5 Modulatory Effects of NAC, H_2O_2, and Colivelin on PPT-Treated OSCC Cells

To investigate the association between PPT and ROS production in OSCC cells, we performed a series of assays. First, 5 mM NAC was applied to HN22 and HSC4 cells for 1 h, and subsequently, they were exposed to 1 μM PPT. The reduction in p-STAT3 levels caused by PPT treatment alone was partially reversed by co-treatment with NAC (Fig. 5A). To confirm these findings, cells were exposed to Colivelin, a STAT3 agonist, and the protein levels were assessed using western blotting to determine whether PPT affected STAT3 activation. The results showed that treatment with Colivelin alone led to an increase in p-STAT3 levels, whereas co-treatment with PPT resulted in a marked reduction in p-STAT3 expression, indicating that PPT effectively counteracted STAT3 activation induced by Colivelin (Fig. 5B). Additionally, Fig. 5C shows that ROS was induced by H_2O_2 treatment, and similar to the PPT-treated group, STAT3 activation was also modulated in the H_2O_2-treated group. These results indicated that PPT plays an important role in inducing apoptosis by directly affecting the STAT3 pathway through ROS regulation (Fig. 6).

4 Discussion

Evasion of apoptosis, a typical characteristic of cancer, is a major mechanism of oncogenesis, cancer development, and resistance to chemotherapy. To overcome this, much research is being conducted; in particular, cell death through ROS-dependent cell death plays an important role in the occurrence and progression of the disease [29,30]. ROS, which naturally forms within cells, are highly reactive molecules containing a single electron and contribute significantly to key physiological activities, such as signal transduction, proliferation, and differentiation. However, when the balance of the antioxidant defense system is disrupted, ROS accumulation triggers oxidative stress. Ultimately, this causes DNA damage and changes in gene expression, leading to various diseases, including cancer, neurodegenerative diseases, aging, and inflammation [31]. Reactive oxygen species are classified into free radicals and non-radicals as follows: hydroxyl radicals, disulfides, superoxide, nitric oxide, and hydrogen peroxide. These species can easily react

with biomolecules and cause cell damage [32]. Hydrogen peroxide, hydroxyl radicals, and superoxide anion species have been extensively studied for their roles in cell signaling and oxidative stress, particularly in cancer [33–35]. As ROS serves as a pivotal factor in the development, progression, and treatment resistance of cancer, researchers are focusing on leveraging this correlation to develop new cancer treatment strategies. This work focused on confirming the anticancer effect of PPT by targeting STAT3 regulation through ROS generation in OSCC cells and elucidating the underlying mechanisms. Our results showed that PPT attenuated cell propagation and colony formation in both the HN22 and HSC4 cell lines and exhibited a cytotoxic effect, leading to cell shrinkage and DNA fragmentation in a dose-dependent manner. Increased ROS within the mitochondria induces apoptosis and can act as a mediator of apoptosis [36]. Accordingly, we assessed the specific role of ROS in PPT-induced apoptosis by flow cytometry using MitoSOX and DCFH-DA dyes.

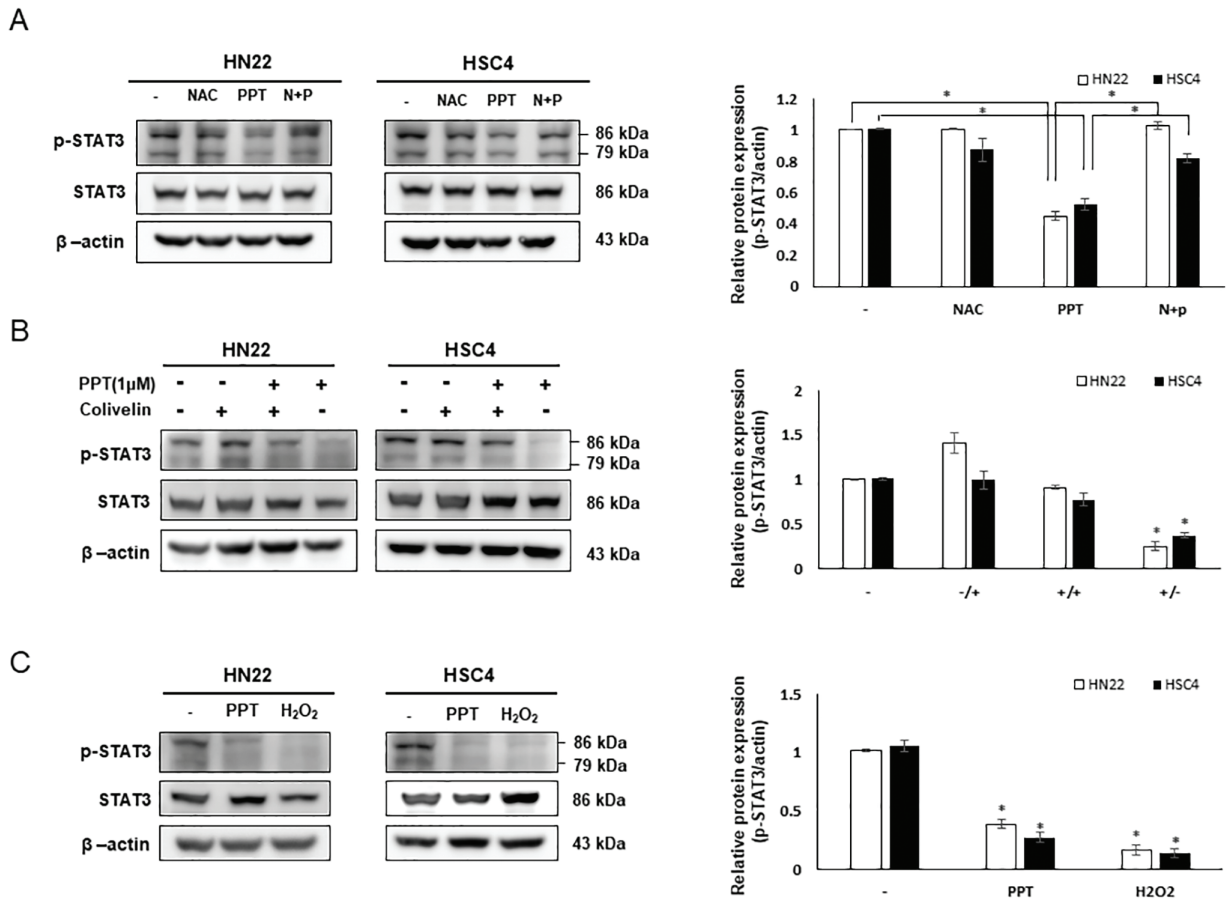

Figure 5: Effect of NAC, STAT3 agonist, and H_2O_2 on p-STAT3 expression in OSCC cells. (A) HN22 and HSC4 cells were pretreated with 5 mM NAC for 1 h or untreated, followed by incubation with 1 μM PPT for 48 h. Cell lysates were analyzed using western blotting to assess p-STAT3, STAT3, and β-actin levels. (B) HN22 and HSC4 cells were pretreated with 5 μM Colivelin for 2 h, followed by exposure to 1 μM PPT for 48 h. The protein levels of STAT3 phosphorylation were quantified and analyzed using western blotting, with β-actin acting as a loading control for normalization. (C) Each cell type was treated with 400 μM H_2O_2 for 48 h to assess the impact on ROS-related STAT3 signaling. Specific antibodies were employed in western blotting to detect protein levels, with β-actin serving as the loading control in this experiment. The bar graph quantifies the proportional p-STAT3 levels (p-STAT3/β-actin) across different treatment groups, showing the mean ± SD (n = 3), and statistical significance is marked as $^*p < 0.05$

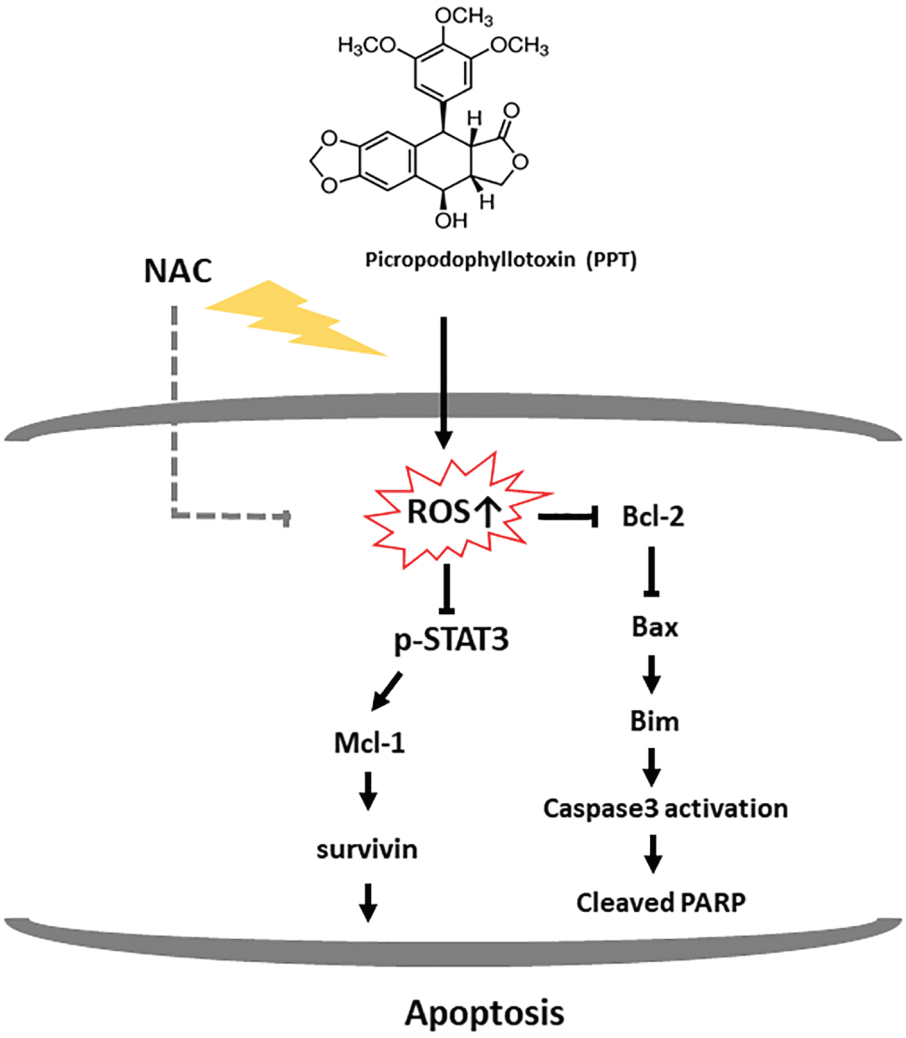

Figure 6: The hypothesized pathway by which PPT exerts its anticancer effects in OSCC cells

In addition, hydrogen peroxide (H_2O_2) is a well-established ROS that rapidly generates ROS within cells, freely diffuses across cellular membranes, and reacts with biomolecules, resulting in oxidative damage and cellular dysfunction. H_2O_2 plays a crucial role in cell signaling, apoptosis, and mitochondrial dysfunction under pathological conditions [37]. In this study, H_2O_2 was utilized as a model system to induce oxidative stress in OSCC cells, mimicking the oxidative damage observed under oxidative stress conditions at the cellular level. Dose-dependent treatment with PPT increased intracellular ROS production. As ROS levels increase, DCFH-DA is oxidized and emits a strong fluorescent signal, a phenomenon reported in various cancer cells through several studies [38–40]. Similarly, our results showed that high-dose PPT significantly increased ROS production, which was effectively blocked in the presence of the ROS scavenger, NAC. NAC is a well-known antioxidant recognized for its ability to directly neutralize ROS and serve as a precursor for intracellular glutathione (GSH) synthesis. Additionally, NAC plays a crucial role in restoring mitochondrial function by preventing ROS-induced mitochondrial membrane depolarization and cell death. It also contributes to maintaining redox equilibrium, a key factor in cell function and survival [41]. The mitochondrial membrane potential is a critical factor that regulates cell survival and death [42,43]. NAC's ability to mitigate ROS and stabilize mitochondrial membrane potential may protect cells from PPT-induced

mitochondrial dysfunction. The findings of this study, based on TMRM analysis, revealed that PPT treatment of OSCC cells weakened the mitochondrial membrane potential, which was associated with mitochondrial collapse and ROS accumulation and could be interpreted as a signal of cancer cell death.

STAT3 is transiently activated under normal conditions; however, its continuous activation in cancer cells confers resistance to apoptosis [44,45]. Consequently, the inhibition of STAT3 signaling reduces cancer cell survival and proliferation, making it a critical target in anticancer treatment strategies explored in numerous studies. Previous studies [46] have demonstrated that ROS can modulate the STAT3 signaling pathway, promoting apoptosis by downregulating anti-apoptotic proteins such as Bcl-2 and survivin. Excessive ROS levels disrupt mitochondrial integrity, leading to the activation of pro-apoptotic markers and facilitating mitochondrial dysfunction. Consistent with these findings, our study shows that ROS generation induced by PPT treatment suppresses STAT3 activation and shifts the balance between pro- and anti-apoptotic proteins, thereby driving apoptosis in OSCC cells. Our study showed that STAT3 activation was progressively inhibited by increasing the dose of PPT in HN22 and HSC4 cells. Consistently, the activation of STAT3, which was suppressed in response to PPT treatment, led to reduced expression of Mcl-1, survivin, Bcl-2, and Bim and increased expression of Bax, c-caspase3, and c-PARP. In particular, the apoptosis indicator, c-PARP, was remarkably elevated in a dose- and time-dependent manner. These findings indicate that PPT facilitates OSCC cell death by suppressing STAT3 activity and modulating the expression of downstream target proteins. In general, STAT3 activation is controlled by upstream signaling molecules, including Janus kinase 2 (JAK2), and various studies have shown that these molecules exhibit simultaneous activation or inhibition [47–49]. Western blotting confirmed that the activation state of JAK2 was assessed after PPT treatment in human OSCC cell lines, but no significant changes were observed (data not shown). In contrast, studies have reported that STAT3 can be activated independently of JAK2 and ROS among various signaling molecules [50]. As evidenced by the findings of this study, combined treatment with NAC and PPT did not suppress STAT3 activation, implying that in OSCC cells, PPT treatment may induce STAT3-independent inactivation via ROS, ultimately triggering cell death. To further investigate this mechanism, we used Colivelin, a synthetic peptide recognized as a potent STAT3 activator that promotes STAT3 phosphorylation and has been widely studied for its neuroprotective effects and its role in cell survival signaling pathways [51]. This aligns with previous findings [46], highlighting the dual role of STAT3 in regulating cell survival and apoptosis. Specifically, ROS's inhibition of STAT3 downregulates cell survival pathways and enhances mitochondrial dysfunction, triggering apoptosis. The use of Colivelin in our study confirmed that STAT3 plays a central role in PPT-induced apoptosis by modulating ROS-mediated signaling. In this study, Colivelin was employed to determine whether STAT3 activation could be restored in OSCC cells following PPT treatment, providing further insight into the ROS-mediated inactivation of STAT3. Notably, co-treatment with the STAT3 activator Colivelin with PPT markedly restored phosphorylated STAT3 expression compared to PPT treatment alone. These results indicate that STAT3 is a major target of PPT and that its anticancer efficacy is predominantly mediated through the inhibition of STAT3 activity. However, our study has certain limitations. First, it was conducted solely through *in vitro* experiments, which limits its applicability to *in vivo* systems. More comprehensive *in vivo* analyses are warranted to validate the findings in a more complex biological environment. Second, the study was limited to two types of cancer cell lines, and further research using diverse cell lines and animal models is needed to confirm the broader applicability of the findings. Although further investigations are necessary to elucidate the intricate interplay between PPT and STAT3, this study constitutes a pioneering report establishing that PPT triggers apoptosis by modulating ROS-mediated STAT3 inactivation in OSCC. In conclusion, the key molecular targets of PPT-induced oral squamous carcinoma cell death were identified to be ROS and STAT3, providing experimental evidence supporting the potential of PPT as a foundation for the development of anticancer therapies.

Acknowledgement: Not applicable.

Funding Statement: This study was supported by the Korea Institute of Toxicology (KIT) Research Program [No. 2710008763 (KK-2401-01)] and the Korea Environmental Industry & Technology Institute (KEITI) through the Core Technology Development Project for Environmental Diseases Prevention and Management [No. 2480000072 (RS-2021-KE001705)].

Author Contributions: The authors confirm their contribution to the paper as follows: study conception and design: Woo-Keun Kim, Young-Joo Jeon; data collection: Jung-Il Chae, Ji-Hye Seo; analysis and interpretation of results: Jung-Il Chae, Ji-Hye Seo, Goo Yoon; draft manuscript preparation: Jung-Il Chae, Ji-Hye Seo; final manuscript revisions and guidance: Woo-Keun Kim, Young-Joo Jeon; compound provision: Goo Yoon. All authors reviewed the results and approved the final version of the manuscript.

Availability of Data and Materials: The datasets generated and analyzed in this study are available from the corresponding author upon reasonable request.

Ethics Approval: Not applicable.

Conflicts of Interest: The authors declare no conflicts of interest to report regarding the present study.

References

1. Fatima J, Fatima E, Mehmood F, Ishtiaq I, Khan MA, Khurshid HMS, et al. Comprehensive analysis of oral squamous cell carcinomas: clinical, epidemiological, and histopathological insights with a focus on prognostic factors and survival time. Cureus. 2024;16(2):e54394. doi:10.7759/cureus.54394.
2. Sung H, Ferlay J, Siegel RL, Laversanne M, Soerjomataram I, Jemal A, et al. Global cancer statistics 2020: globocan estimates of incidence and mortality worldwide for 36 cancers in 185 countries. CA Cancer J Clin. 2021;71(3):209–49. doi:10.3322/caac.21660.
3. Tan Y, Wang Z, Xu M, Li B, Huang Z, Qin S, et al. Oral squamous cell carcinomas: state of the field and emerging directions. Int J Oral Sci. 2023;15(1):44. doi:10.1038/s41368-023-00249-w.
4. Chamoli A, Gosavi AS, Shirwadkar UP, Wangdale KV, Behera SK, Kurrey NK, et al. Overview of oral cavity squamous cell carcinoma: risk factors, mechanisms, and diagnostics. Oral Oncol. 2021;121(3):105451. doi:10.1016/j.oraloncology.2021.105451.
5. Zheng J, Chen K, Cai L, Pan Y, Zeng Y. A potential biomarker for the early diagnosis of OSCC: saliva and serum PrP^{C}. J Cancer. 2024;15(6):1593–602. doi:10.7150/jca.92489.
6. Feng X, Xiao L. Galectin 2 regulates JAK/STAT3 signaling activity to modulate oral squamous cell carcinoma proliferation and migration *in vitro*. BIOCELL. 2024;48(5):793–801. doi:10.32604/biocell.2024.048395.
7. Neophytou CM, Trougakos IP, Erin N, Papageorgis P. Apoptosis deregulation and the development of cancer multi-drug resistance. Cancers. 2021;13(17):4363. doi:10.3390/cancers13174363.
8. Lan YY, Cheng TC, Lee YP, Wang CY, Huang BM. Paclitaxel induces human KOSC3 oral cancer cell apoptosis through caspase pathways. BIOCELL. 2024;48(7):1047–54. doi:10.32604/biocell.2024.050701.
9. Lee JY, Kang BY, Jung SJ, Kwak AW, Lee SO, Park JW, et al. Picropodophyllotoxin inhibits cell growth and induces apoptosis in gefitinib-resistant non-small lung cancer cells by dual-targeting EGFR and MET. Biomol Ther. 2023;31(2):200–9. doi:10.4062/biomolther.2022.113.
10. Lee SO, Kwak AW, Lee MH, Seo JH, Cho SS, Yoon G, et al. Picropodophyllotoxin induces G1 cell cycle arrest and apoptosis in human colorectal cancer cells via ROS generation and activation of p38 MAPK signaling pathway. J Microbiol Biotechnol. 2021;31(12):1615–23. doi:10.4014/jmb.2109.09012.
11. Kwak AW, Yoon G, Lee MH, Cho SS, Shim JH, Chae JI. Picropodophyllotoxin, an epimer of podophyllotoxin, causes apoptosis of human esophageal squamous cell carcinoma cells through ROS-mediated JNK/P38 MAPK pathways. Int J Mol Sci. 2020;21(13):4640. doi:10.3390/ijms21134640.

12. Weidemüller P, Kholmatov M, Petsalaki E, Zaugg JB. Transcription factors: bridge between cell signaling and gene regulation. Proteomics. 2021;21(23–4):e2000034. doi:10.1002/pmic.202000034.
13. Wingender E, Schoeps T, Dönitz J. TFClass: an expandable hierarchical classification of human transcription factors. Nucleic Acids Res. 2013;41(D1):D165–70. doi:10.1093/nar/gks1123.
14. Patel N, Bush WS. Modeling transcriptional regulation using gene regulatory networks based on multi-omics data sources. BMC Bioinformatics. 2021;22(1):200. doi:10.1186/s12859-021-04126-3.
15. Lambert SA, Jolma A, Campitelli LF, Das PK, Yin Y, Albu M, et al. The human transcription factors. Cell. 2018;172(4):650–65. doi:10.1016/j.cell.2018.01.029.
16. Wang HQ, Man QW, Huo FY, Gao X, Lin H, Li SR, et al. STAT3 pathway in cancers: past, present, and future. MedComm. 2022;3(2):e124. doi:10.1002/mco2.124.
17. Tolomeo M, Cascio A. The multifaced role of STAT3 in cancer and its implication for anticancer therapy. Int J Mol Sci. 2021;22(2):603. doi:10.3390/ijms22020603.
18. Diaz N, Minton S, Cox C, Bowman T, Gritsko T, Garcia R, et al. Activation of Stat3 in primary tumors from high-risk breast cancer patients is associated with elevated levels of activated SRC and survivin expression. Clin Cancer Res. 2006;12(1):20–8. doi:10.1158/1078-0432.CCR-04-1749.
19. Kang JH, Jang YS, Lee HJ, Lee CY, Shin DY, Oh SH. Inhibition of STAT3 signaling induces apoptosis and suppresses growth of lung cancer: Good and bad. Lab Anim Res. 2019;35(1):30. doi:10.1186/s42826-019-0030-0.
20. Park YR, Jee W, Park SM, Kim SW, Bae H, Jung JH, et al. *Viscum album* induces apoptosis by regulating STAT3 signaling pathway in breast cancer cells. Int J Mol Sci. 2023;24(15):11988. doi:10.3390/ijms241511988.
21. Kim DY, Cha ST, Ahn DH, Kang HY, Kwon CI, Ko KH, et al. STAT3 expression in gastric cancer indicates a poor prognosis. J Gastro Hepatol. 2009;24(4):646–51. doi:10.1111/j.1440-1746.2008.05671.x.
22. Wang YX, Cai H, Jiang G, Zhou TB, Wu H. Silibinin inhibits proliferation, induces apoptosis and causes cell cycle arrest in human gastric cancer MGC803 cells via STAT3 pathway inhibition. Asian Pac J Cancer Prev. 2014;15(16):6791–8. doi:10.7314/apjcp.2014.15.16.6791.
23. Cai Q, Lin J, Wei L, Zhang L, Wang L, Zhan Y, et al. *Hedyotis* diffusa Willd inhibits colorectal cancer growth *in vivo* via inhibition of STAT3 signaling pathway. Int J Mol Sci. 2012;13(5):6117–28. doi:10.3390/ijms13056117.
24. Morikawa T, Baba Y, Yamauchi M, Kuchiba A, Nosho K, Shima K, et al. STAT3 expression, molecular features, inflammation patterns, and prognosis in a database of 724 colorectal cancers. Clin Cancer Res. 2011;17(6):1452–62. doi:10.1158/1078-0432.CCR-10-2694.
25. Maggioni D, Garavello W, Rigolio R, Pignataro L, Gaini R, Nicolini G. Apigenin impairs oral squamous cell carcinoma growth *in vitro* inducing cell cycle arrest and apoptosis. Int J Oncol. 2013;43(5):1675–82. doi:10.3892/ijo.2013.2072.
26. Biswal S, Panda M, Biswal BK. Shikonin stimulates mitochondria-mediated apoptosis by enhancing intracellular reactive oxygen species production and DNA damage in oral cancer cells. J Cell Biochem. 2025;126(1):e30671. doi:10.1002/jcb.30671.
27. Deng XS, Wang S, Deng A, Liu B, Edgerton SM, Lind SE, et al. Metformin targets Stat3 to inhibit cell growth and induce apoptosis in triple-negative breast cancers. Cell Cycle. 2012;11(2):367–76. doi:10.4161/cc.11.2.18813.
28. Mora LB, Buettner R, Seigne J, Diaz J, Ahmad N, Garcia R, et al. Constitutive activation of STAT3 in human prostate tumors and cell lines: Direct inhibition of STAT3 signaling induces apoptosis of prostate cancer cells. Cancer Res. 2002;62(22):6659–66.
29. Zhao Y, Ye X, Xiong Z, Ihsan A, Ares I, Martínez M, et al. Cancer metabolism: the role of ROS in DNA damage and induction of apoptosis in cancer cells. Metabolites. 2023;13(7):796. doi:10.3390/metabo13070796.
30. Renschler MF. The emerging role of reactive oxygen species in cancer therapy. Eur J Cancer. 2004;40(13):1934–40. doi:10.1016/j.ejca.2004.02.031.
31. Hajam YA, Rani R, Ganie SY, Sheikh TA, Javaid D, Qadri SS, et al. Oxidative stress in human pathology and aging: molecular mechanisms and perspectives. Cells. 2022;11(3):552. doi:10.3390/cells11030552.
32. Hassan HA, Ahmed HS, Hassan DF. Free radicals and oxidative stress: mechanisms and therapeutic targets. Hum Antibodies. 2024;32(4):151–67. doi:10.3233/HAB-240011.

33. Knickle A, Fernando W, Greenshields AL, Vasantha Rupasinghe HP, Hoskin DW. Myricetin-induced apoptosis of triple-negative breast cancer cells is mediated by the iron-dependent generation of reactive oxygen species from hydrogen peroxide. Food Chem Toxicol. 2018;118:154–67. doi:10.1016/j.fct.2018.05.005.
34. Iwasaki K, Zheng YW, Murata S, Ito H, Nakayama K, Kurokawa T, et al. Anticancer effect of linalool via cancer-specific hydroxyl radical generation in human colon cancer. World J Gastroenterol. 2016;22(44):9765–74. doi:10.3748/wjg.v22.i44.9765.
35. Xu L, Wu T, Lu S, Hao X, Qin J, Wang J, et al. Mitochondrial superoxide contributes to oxidative stress exacerbated by DNA damage response in RAD51-depleted ovarian cancer cells. Redox Biol. 2020;36:101604. doi:10.1016/j.redox.2020.101604.
36. Fleury C, Mignotte B, Vayssière JL. Mitochondrial reactive oxygen species in cell death signaling. Biochimie. 2002;84(2–3):131–41. doi:10.1016/s0300-9084(02)01369-x.
37. Sarmiento-Salinas FL, Perez-Gonzalez A, Acosta-Casique A, Ix-Ballote A, Diaz A, Treviño S, et al. Reactive oxygen species: role in carcinogenesis, cancer cell signaling and tumor progression. Life Sci. 2021;284(6):119942. doi:10.1016/j.lfs.2021.119942.
38. Zhao Z, Wang Y, Gong Y, Wang X, Zhang L, Zhao H, et al. Celastrol elicits antitumor effects by inhibiting the STAT3 pathway through ROS accumulation in non-small cell lung cancer. J Transl Med. 2022;20(1):525. doi:10.1186/s12967-022-03741-9.
39. Fan X, Xie M, Zhao F, Li J, Fan C, Zheng H, et al. Daphnetin triggers ROS-induced cell death and induces cytoprotective autophagy by modulating the AMPK/Akt/mTOR pathway in ovarian cancer. Phytomedicine. 2021;82:153465. doi:10.1016/j.phymed.2021.153465.
40. Syed FQ, Elkady AI, Mohammed FA, Mirza MB, Hakeem KR, Alkarim S. Chloroform fraction of *Foeniculum* vulgare induced ROS mediated, mitochondria-caspase-dependent apoptotic pathway in MCF-7, human breast cancer cell line. J Ethnopharmacol. 2018;218(48):16–26. doi:10.1016/j.jep.2018.02.029.
41. Raghu G, Berk M, Campochiaro PA, Jaeschke H, Marenzi G, Richeldi L, et al. The multifaceted therapeutic role of N-acetylcysteine (NAC) in disorders characterized by oxidative stress. Curr Neuropharmacol. 2021;19(8):1202–24. doi:10.2174/18756190MTEycODQ8w.
42. Düssmann H, Rehm M, Kögel D, Prehn JHM. Outer mitochondrial membrane permeabilization during apoptosis triggers caspase-independent mitochondrial and caspase-dependent plasma membrane potential depolarization: a single-cell analysis. J Cell Sci. 2003;116(Pt 3):525–36. doi:10.1242/jcs.00236.
43. Kuwahara Y, Tomita K, Roudkenar MH, Roushandeh AM, Urushihara Y, Igarashi K, et al. Decreased mitochondrial membrane potential is an indicator of radioresistant cancer cells. Life Sci. 2021;286(2):120051. doi:10.1016/j.lfs.2021.120051.
44. Tesoriere A, Dinarello A, Argenton F. The roles of post-translational modifications in STAT3 biological activities and functions. Biomedicines. 2021;9(8):956. doi:10.3390/biomedicines9080956.
45. El-Tanani M, Al Khatib AO, Aladwan SM, Abuelhana A, McCarron PA, Tambuwala MM. Importance of STAT3 signalling in cancer, metastasis and therapeutic interventions. Cell Signal. 2022;92(6):110275. doi:10.1016/j.cellsig.2022.110275.
46. Li L, Li W, Liu Y, Jin X, Yu Y, Lin H. TBBPA and lead co-exposure induces grass carp liver cells apoptosis via ROS/JAK2/STAT3 signaling axis. Fish Shellfish Immunol. 2023;142(6):109100. doi:10.1016/j.fsi.2023.109100.
47. Saleem MZ, Nisar MA, Alshwmi M, Din SRU, Gamallat Y, Khan M, et al. Brevilin A inhibits STAT3 signaling and induces ROS-dependent apoptosis, mitochondrial stress and endoplasmic reticulum stress in MCF-7 breast cancer cells. Onco Targets Ther. 2020;13:435–50. doi:10.2147/OTT.
48. Yin W, Fu X, Chang W, Han L, Meng J, Cao A, et al. Antiovarian cancer mechanism of esculetin: inducing G0/G1 arrest and apoptosis via JAK2/STAT3 signalling pathway. J Pharm Pharmacol. 2023;75(1):87–97. doi:10.1093/jpp/rgac083.
49. Kim BI, Kim JH, Sim DY, Nam M, Jung JH, Shim B, et al. Inhibition of JAK2/STAT3 and activation of caspase-9/3 are involved in KYS05090S-induced apoptosis in ovarian cancer cells. Int J Oncol. 2019;55(1):203–10. doi:10.3892/ijo.2019.4795.

50. Li L, Chen M, Li G, Cai R. Raddeanin A induced apoptosis of non-small cell lung cancer cells by promoting ROS-mediated STAT3 inactivation. Tissue Cell. 2021;71:101577. doi:10.1016/j.tice.2021.101577.
51. Chiba T, Yamada M, Sasabe J, Terashita K, Aiso S, Matsuoka M, et al. Colivelin prolongs survival of an ALS model mouse. Biochem Biophys Res Commun. 2006;343(3):793–8. doi:10.1016/j.bbrc.2006.02.184.